ELSEVIER

Journal of Biomechanics 36 (2003) 803–813

JOURNAL OF BIOMECHANICS

www.elsevier.com/locate/jbiomech
www.JBiomech.com

Non-driving intersegmental knee moments in cycling computed using a model that includes three-dimensional kinematics of the shank/foot and the effect of simplifying assumptions

Colin S. Gregersen[a], M.L. Hull[a,b,*]

[a] *Biomedical Engineering Program, University of California, Davis, CA 95616, USA*
[b] *Department of Mechanical Engineering, University of California, Davis, CA 95616, USA*

Accepted 19 December 2002

Abstract

Assessing the importance of non-driving intersegmental knee moments (i.e. varus/valgus and internal/external axial moments) on over-use knee injuries in cycling requires the use of a three-dimensional (3-D) model to compute these loads. The objectives of this study were: (1) to develop a complete, 3-D model of the lower limb to calculate the 3-D knee loads during pedaling for a sample of the competitive cycling population, and (2) to examine the effects of simplifying assumptions on the calculations of the non-driving knee moments. The non-driving knee moments were computed using a complete 3-D model that allowed three rotational degrees of freedom at the knee joint, included the 3-D inertial loads of the shank/foot, and computed knee loads in a shank-fixed coordinate system. All input data, which included the 3-D segment kinematics and the six pedal load components, were collected from the right limb of 15 competitive cyclists while pedaling at 225 W and 90 rpm. On average, the peak varus and internal axial moments of 7.8 and 1.5 N m respectively occurred during the power stroke whereas the peak valgus and external axial moments of 8.1 and 2.5 N m respectively occurred during the recovery stroke. However, the non-driving knee moments were highly variable between subjects; the coefficients of variability in the peak values ranged from 38.7% to 72.6%. When it was assumed that the inertial loads of the shank/foot for motion out of the sagittal plane were zero, the root-mean-squared difference (RMSD) in the non-driving knee moments relative to those for the complete model was 12% of the peak varus/valgus moment and 25% of the peak axial moment. When it was also assumed that the knee joint was revolute with the flexion/extension axis perpendicular to the sagittal plane, the RMSD increased to 24% of the peak varus/valgus moment and 204% of the peak axial moment. Thus, the 3-D orientation of the shank segment has a major affect on the computation of the non-driving knee moments, while the inertial contributions to these loads for motions out of the sagittal plane are less important.

1. Introduction

Over-use injury in cycling is commonly manifest at the knee joint where, over time, knee joint structures become damaged from low-level repetitive loading (Holmes et al., 1991). Determining the force and moment components transmitted by the knee during cycling is useful to understand the etiology of over-use injury and also to assess the effectiveness of different interventions to protect against over-use injury. Because the loads thought to be primarily responsible for over-use knee injury are the non-driving moments (varus/valgus and internal/external axial moments) transmitted by the knee (Francis, 1986), a three-dimensional (3-D) model is necessary for calculating these loads.

To our knowledge, calculations of the non-driving knee moments have been limited to two studies. Performed by Ericson et al. (1984), the first study developed a frontal plane model where the varus/valgus knee moment was calculated using only the normal and medial/lateral pedal forces. While serving as the first step in calculating the varus/valgus knee moment, this model neglected the abduction/adduction and inversion/eversion pedal moment contributions to the varus/valgus knee moment, which are not insignificant (Davis and Hull, 1981). Performed by Ruby et al. (1992a), the

*Corresponding author. Tel.: +1-530-752-6220; fax: +1-530-752-4158.
E-mail address: mlhull@ucdavis.edu (M.L. Hull).

0021-9290/03/$ - see front matter © 2003 Elsevier Science Ltd. All rights reserved.
doi:10.1016/S0021-9290(03)00014-9

second study combined results from two, 2-D knee models to calculate the 3-D knee loads. This study demonstrated the importance of measuring all six load components at the pedal and their cumulative effects on non-driving knee loads.

In demonstrating the contribution of all pedal load components to knee loads, Ruby et al. assumed that inertial contributions to the knee loads resulting from motion out of the sagittal plane were negligible and that the knee joint was revolute. Because relaxing these assumptions may affect computed knee loads to some degree, it would be advantageous to use a 3-D model that includes complete 3-D kinematics of the shank to examine the effects of these assumptions on the non-driving moment calculations. Therefore, there were two objectives of this study. The first objective was to develop a complete 3-D model of the lower limb to calculate the 3-D knee loads during pedaling for a sample of the competitive cycling population. The second objective was to examine the effects of simplifying assumptions on the calculations of the non-driving knee moments.

2. Methods

2.1. Analytic model

An inverse dynamics approach was utilized to calculate the 3-D knee loads during pedaling. The lower limb segments were modeled as rigid bodies interconnected by spherical joints. The intersegmental loads were calculated at the center of these joints. For each segment, the distal forces, distal moments, kinetics, and kinematics were used to determine the unknown proximal loads. The proximal loads were calculated from

$$\mathbf{F}_p = m_s \mathbf{a}^{s^*} - \mathbf{F}_d - \mathbf{F}_g, \tag{1}$$

$$\mathbf{M}_p = \dot{\mathbf{H}}^{s/s^*} - \mathbf{M}_d - (\mathbf{r}^{p/s^*} \times \mathbf{F}_p) - (\mathbf{r}^{d/s^*} \times \mathbf{F}_d), \tag{2}$$

where $\mathbf{F}_p$, $\mathbf{F}_g$, and $\mathbf{F}_d$ are the respective proximal, gravitational, and distal force vectors, m_s is the segment mass, $\boldsymbol{a}^{s^*}$ is the acceleration vector of the segment center of mass (denoted by s*), $\mathbf{M}_p$ and $\mathbf{M}_d$ are the respective proximal and distal moment vectors about the center of mass, $\mathbf{r}^{p/s^*}$ and $\mathbf{r}^{d/s^*}$ are the position vectors to the respective proximal and distal joint centers from the segment center of mass, and $\dot{\mathbf{H}}^{s/s^*}$ is the time derivative of the angular momentum vector of the segment about its center of mass (expressed in the segment-fixed principal basis) (Fig. 1). With the principal directions and principal moments of inertia ($I_{x^*x^*}$, $I_{y^*y^*}$, $I_{z^*z^*}$) known, the components of the angular momentum vector $\dot{\mathbf{H}}^{s/s^*}$ were determined as

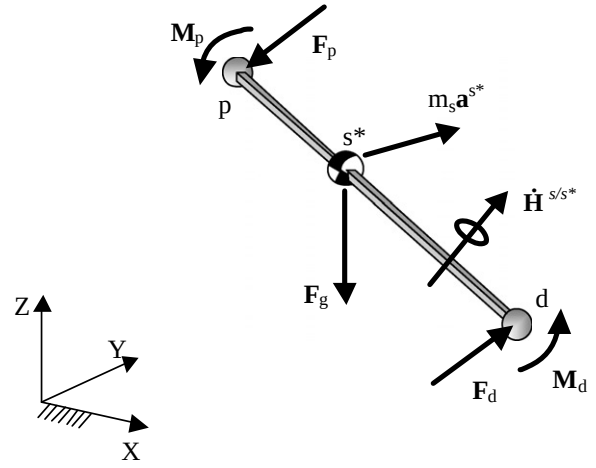

Fig. 1. Generic three-dimensional body segment containing distal (d) joint center, proximal (p) joint center, and center of mass (s*) points. See text for definitions of vectors.

$$\begin{aligned}
\dot{H}_{x^*}^{s/s^*} &= I_{x^*x^*}\dot{\omega}_{x^*} - (I_{y^*y^*} - I_{z^*z^*})\omega_{y^*}\omega_{z^*},\\
\dot{H}_{y^*}^{s/s^*} &= I_{y^*y^*}\dot{\omega}_{y^*} - (I_{z^*z^*} - I_{x^*x^*})\omega_{z^*}\omega_{x^*},\\
\dot{H}_{z^*}^{s/s^*} &= I_{z^*z^*}\dot{\omega}_{z^*} - (I_{x^*x^*} - I_{y^*y^*})\omega_{x^*}\omega_{y^*},
\end{aligned} \tag{3}$$

where ω_{x^*}, ω_{y^*}, and ω_{z^*} are the scalar components of the angular velocity vector of the segment expressed in the principal basis (x^*, y^*, z^*), and $\dot{\omega}_{x^*}$, $\dot{\omega}_{y^*}$, and $\dot{\omega}_{z^*}$ are the scalar components of the time derivative of the angular velocity vector expressed in the principal basis. Using the external pedal load vectors as $\mathbf{M}_d$ and $\mathbf{F}_d$ for the foot segment, the proximal intersegmental ankle load vectors were calculated. The reaction vectors were then used as $\mathbf{M}_d$ and $\mathbf{F}_d$ for the shank segment to calculate the proximal intersegmental knee load vectors. All kinetic and kinematic model inputs in Eqs. (1) and (2) were measured directly from each subject.

2.2. Model inputs

The distal force and moment vectors ($\mathbf{F}_d$ and $\mathbf{M}_d$, respectively) applied to the foot were measured with a six-load component pedal dynamometer (Model PD-001, Shimano Industrial Corporation, Osaka, Japan). This dynamometer had maximum root-mean-squared error (RMSE) values of 7.1, 1.7, and 2.6 N for the respective x, y, and z pedal force components, and 0.16, 0.04, and 0.34 N m for the respective x, y, and z moments (Ruby and Hull, 1993). All external forces and moments were calculated at the pedal reference point (origin of the pedal local coordinate system) defined as the intersection between the symmetry axis of the clipless pedal contact surface and a line perpendicular from this surface to the pedal spindle axis.

The remaining kinematic and kinetic quantities necessary to solve for the intersegmental knee loads using Eqs. (1) and (2) were determined in three steps.

The first step was to determine the position vectors to the joint centers from the origin of an intermediate, marker-based local coordinate system, expressed in the intermediate basis. Reflective markers were mounted on the subject's heel, toe, lateral malleolus, medial malleolus, tibial tuberosity, lateral epicondyle, and medial epicondyle. In addition, three reflective markers were mounted on the pedal body (Fig. 2). The heel marker was mounted over the cycling shoe to represent the posterior-most point on the heel. Similarly, the toe marker was mounted to represent the tip of the longest toe (first or second).

Following marker placement, a static calibration trial was recorded for 1 s using a video-based motion capture system (Motion Analysis Inc., Santa Rosa, CA). During this trial, the subject rested the right foot on the pedal with the ankle and knee joints at approximately 90° of flexion. The static calibration trial was necessary to determine the position vectors to the ankle joint center (AJC) and knee joint center (KJC) from intermediate local coordinate system origins expressed in the intermediate local basis, which were used for the subsequent pedaling trials to track the AJC and KJC.

Using the three pedal markers, a local pedal coordinate system (Fig. 2) was established and the transformation matrix between the laboratory and pedal bases was determined. The position vector to the pedal reference point from the local pedal origin was measured directly and expressed in the local pedal basis. The position vector to the pedal reference point from the laboratory origin was determined.

Intermediate local coordinate systems were established on both the foot and shank using a virtual marker in conjunction with two segment-fixed markers (Ramakrishnan et al., 1987). The intermediate local coordinate system on the foot was established using the virtual reference point on the pedal in conjunction with the heel (origin) and toe markers. The AJC was assumed to lie midway along a line connecting the medial and lateral malleoli markers. The position vector to the AJC from the local origin was determined and expressed in the intermediate foot basis. A position vector to the AJC from the laboratory origin, expressed in the laboratory basis, was also calculated. The coordinates of this vector were used as a virtual marker for the AJC.

Similarly an intermediate, local coordinate system was established on the shank using the virtual AJC in conjunction with the lateral malleolus (origin) and tibial tuberosity markers. The KJC was assumed to lie midway along a line connecting the epicondyle markers. The position vector to the KJC from the local origin was determined and expressed in the intermediate segment basis. A position vector to the KJC from the laboratory origin, expressed in the laboratory basis, was also calculated. The coordinates of this vector were used as a virtual marker for the KJC. Defining the two position vectors to the joint centers from the intermediate local coordinate system origins was necessary because the medial malleolus and medial epicondyle markers would not clear the bicycle frame during the pedaling trials and had to be removed following the static calibration.

The second step in determining the kinematic and kinetic inputs was to determine the position vectors to the joint centers from the laboratory coordinate system origin in the pedaling trials, express them in the laboratory basis, and develop the principal bases. For the foot segment, this position vector to the AJC from the laboratory origin was determined for all foot

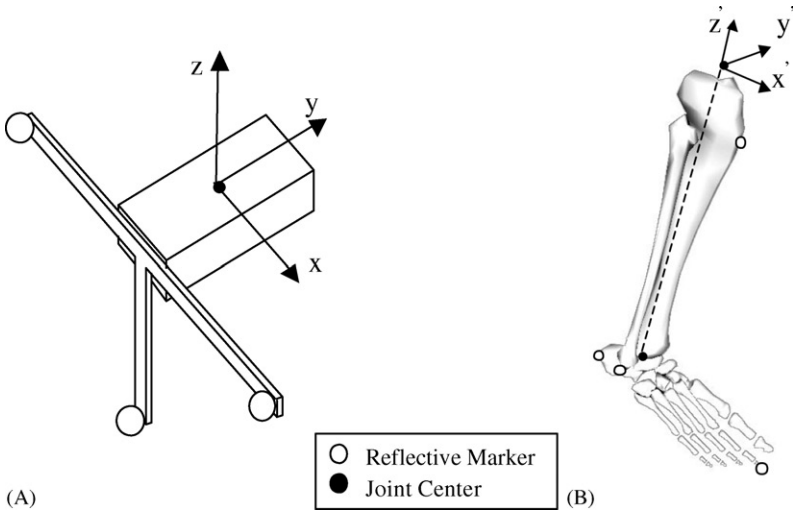

Fig. 2. (A) Illustration of pedal dynamometer reflective markers and local pedal coordinate system. The origin of the local pedal coordinate system coincides with the pedal reference point. (B) Illustration of lower limb reflective markers and virtual joint centers for the ankle and knee joints. The knee joint center served as the origin of the local shank coordinate system in which the knee load components were computed.

positions during the pedaling trials as described above. The foot principal coordinate system was established using the AJC, heel, and toe markers and the transformation between the laboratory coordinate system and the principal coordinate system was determined. For the foot principal coordinate system, the anterior/posterior x-axis was the line connecting the heel and toe markers (anterior positive), the proximal/distal z-axis was perpendicular to the anterior/posterior axis passing through the AJC (proximal direction positive), and the medial/lateral y-axis was mutually perpendicular to these axes. Note that these directions correspond to the respective longitudinal, frontal, and sagittal directions described by Zatsiorsky et al. (1990) and used by de Leva (1996) in determining mass and moment of inertia parameters. The position vector to the foot center of mass (origin of the principal basis) from the laboratory origin was calculated based on the position vector to the heel from the laboratory origin and a percentage along the line connecting both the heel and toe markers (de Leva, 1996).

The shank principal coordinate system was determined similarly where the position vectors to the AJC, KJC, and tibial tuberosity from the laboratory origin were used. Again, the directions of the principal axes were based on de Leva (1996) where the proximal/distal z-axis connected the joint centers (proximal positive), the anterior/posterior x-axis was perpendicular to this axis passing through the tibial tuberosity (anterior positive), and the medial/lateral y-axis was mutually perpendicular to these two axes. These directions correspond to the respective longitudinal, sagittal, and transverse directions (de Leva, 1996). The position vector to the shank center of mass was calculated based on the position vector to the KJC from the laboratory origin and a percentage along a line connecting the AJC and KJC virtual markers.

The third and final step involved calculating the necessary kinematic and kinetic inputs in Eqs. (1) and (2) to solve for the intersegmental load vectors. For the foot, $\boldsymbol{a}^{s*}$ was determined by taking the second time derivative of the position vector to the foot center of mass from the laboratory origin using finite difference methods. The mass of the foot was estimated (de Leva, 1996). Eq. (1) was then solved for the ankle joint intersegmental force vector, expressed in the foot principal basis. The position vectors to the pedal reference point and to the AJC from the foot center of mass ($\mathbf{r}^{d/s*}$ and $\mathbf{r}^{p/s*}$) were then determined and were expressed in the foot principal basis. The cross products of these vectors with the respective pedal force vector ($\mathbf{F}_d$) and intersegmental ankle force vector ($\mathbf{F}_p$) were then calculated. The kinematic inputs for Eq. (3) were then determined where the angular velocity vector of the segment in the laboratory basis ($^N\boldsymbol{\omega}^S$) was calculated from

$$^N\boldsymbol{\omega}^S = \left(\frac{^N\mathrm{d}(\mathbf{j}^*)}{\mathrm{d}t}\bullet\mathbf{k}^*\right)\mathbf{i}^* + \left(\frac{^N\mathrm{d}(\mathbf{k}^*)}{\mathrm{d}t}\bullet\mathbf{i}^*\right)\mathbf{j}^* + \left(\frac{^N\mathrm{d}(\mathbf{i}^*)}{\mathrm{d}t}\bullet\mathbf{j}^*\right)\mathbf{k}^*, \quad (4)$$

where $\mathbf{i}^*, \mathbf{j}^*$, and $\mathbf{k}^*$ are the unit vectors of the principal basis. Given a generic transformation matrix to the laboratory basis N from the principal basis P such as

$$[T]^{N/P} = \begin{bmatrix} a_{11} & a_{12} & a_{13} \\ a_{21} & a_{22} & a_{23} \\ a_{31} & a_{32} & a_{33} \end{bmatrix}, \quad (5)$$

the x^*, y^*, and z^* components of the angular velocity vector of a given segment relative to the laboratory reference frame and expressed in the principal basis become

$$\begin{aligned} ^N\omega^S_{x^*} &= \dot{a}_{12}a_{13} + \dot{a}_{22}a_{23} + \dot{a}_{32}a_{33}, \\ ^N\omega^S_{y^*} &= \dot{a}_{13}a_{11} + \dot{a}_{23}a_{21} + \dot{a}_{33}a_{31}, \\ ^N\omega^S_{z^*} &= \dot{a}_{11}a_{12} + \dot{a}_{21}a_{22} + \dot{a}_{31}a_{32}, \end{aligned} \quad (6)$$

and the angular acceleration components are the time derivatives of these components. The principal inertia tensor for the foot segment was estimated (de Leva, 1996), after which Eq. (2) was solved for the ankle joint intersegmental moment vector, expressed in the principal basis. For the shank, the same procedure was followed to calculate the kinematic and kinetic inputs to solve for the knee intersegmental force and moment vectors, expressed in the shank principal basis.

Knee loads were expressed in a shank-fixed coordinate system (Fig. 2) where the axes reflected the functional axes of the knee joint (Hollister et al., 1993) while remaining necessarily orthogonal. The z'-axis was the line that connected the knee joint center to the ankle joint center. The x' and y' axes were located in a plane perpendicular to the z'-axis, where the y'-axis was the projection of the knee flexion/extension axis onto this plane (medial direction positive). The x'-axis was mutually perpendicular to the two (anterior direction positive). These axes represented the internal/external axial (z'), flexion/extension (y'), and varus/valgus (x') axes of the knee joint. This coordinate system was defined in the static calibration trial, where the transformation matrix to this coordinate system from the principal coordinate system was calculated as a simple rotation about the principal proximal/distal axis. Intersegmental knee loads were expressed as loads applied to the tibia that must be equilibrated by structures crossing the knee (i.e. muscles, ligaments, and bones). This convention is interpreted as tendencies for relative motion of the tibia with respect to the femur. Hence, a positive $M_{y'}$ would act to flex the knee joint (applied flexion moment), a positive $M_{x'}$ would cause the tibia to adduct relative to the femur (applied varus

moment), and a positive $M_{z'}$ would cause the tibia to rotate internally relative to the femur (applied internal axial moment).

2.3. Simplified models

Two other models were developed to examine how simplifying assumptions affect the calculation of the 3-D knee loads. One of these two models, termed the simplified spherical joint model, was identical to the complete spherical joint model described above except that the mass and moments of inertia of the foot, the moments of inertia of the shank about the x^* and z^* principal axes, and the medial/lateral accelerations of the shank were all zero. The second of these two models, termed the revolute joint model, was the same as the simplified spherical joint model, except that the knee joint was assumed revolute with the axis of revolution y' coincident with the laboratory y-axis (medial/lateral direction) (Ruby et al., 1992a). The z'-axis was perpendicular to the y'-axis and passed through the ankle and knee joint centers, and the x'-axis was mutually perpendicular to both.

2.4. Experiment

Fifteen competitive cyclists, none of whom had a history of over-use knee injury in cycling, volunteered to participate in the study. The average age of the subjects was 28 ± 4 years (mean ± 1 S.D.), range 18–30 years; average height was 1.82 ± 0.06 m, range 1.73–1.91 m; and average mass was 77.7 ± 8.3 kg, range 65.8–95.3 kg. The subjects pedaled a conventional racing bicycle mounted on an electronically braked Velodyne ergometer (Frontline Technology, Inc., Irvine, CA) that allowed a constant workrate to be set independent of pedaling rate. The subjects adjusted the bicycle to match their own bicycle's geometry. The subjects all used zero-float clipless pedals and were allowed to choose their own cleat angle. Data were collected from the right leg.

Three markers attached to the bicycle were used to establish a frame-fixed coordinate system in order to track the position of a virtual marker located at the point connecting the crank arm to the crank spindle. Another virtual marker was also developed to track the point connecting the pedal spindle to the crank. These markers allowed the crank angle to be computed. Crank angle was defined as zero when the crank was vertical and upward (top-dead-center position). The virtual crank center marker position was calculated using a static calibration trial, identical to the static calibration trial for the subject, where a reflective marker was attached to the crank center point. The virtual pedal spindle marker position was measured directly in the pedal-fixed basis.

The reflective marker position-time data were collected and processed utilizing a motion capture system (Motion Analysis Inc., Santa Rosa, CA). Four high-speed video cameras were placed in an umbrella arrangement such that the 3-D marker positions were recorded. The dynamometer output was synchronized, and collected by the motion capture system. The camera sampling frequency was 120 Hz, while the sampling of the dynamometer outputs was 1200 Hz. The 12-bit A/D board contained in the motion analysis system digitized the analog inputs. The strain gage amplifier (Measurements Group, Raleigh, NC) gains for the dynamometer were set to yield maximum resolution of the digitized signal, yet eliminate any possible signal saturation. Prior to testing, the motion capture system and bicycle ergometer were calibrated and the pedal dynamometer offset values were recorded. All the reflective markers outlined above were attached to the subject and bicycle. For all subjects, the markers remained in place for the duration of the study. Following marker placement, the static calibration trial was performed to determine joint center locations. Pedal dynamometer and marker path data were filtered using a second-order, zero phase shift low-pass Butterworth filter with a cutoff frequency of 6 Hz (Winter, 1990). The testing protocol consisted of a 15-min warm-up period at a workrate of 100 W and cadence of 90 rpm. Following the warm-up period, experimental data were recorded while the subject pedaled at a workrate of 225 W and 90 rpm for 5 min in a 52×19 gear. Four, 5 s trials were recorded during this period, yielding approximately 30 cycles of data.

The x', y', and z' load components of the intersegmental force and moment vectors at the knee were computed as a function of crank angle. The load components for all complete pedal revolutions for each subject were linearly interpolated in 5° increments of the crank angle (effective reduction of sampling frequency to 96 Hz) and an average load component–angle curve was generated for all of the subjects. For the calculations of knee loads using the complete spherical joint model, the maximum number of complete pedal cycles (22–30) obtained during the recording session was used to compute the average load component–angle curve for each subject.

Comparisons between the two simplified models (simplified spherical joint and revolute joint) and the complete spherical model were performed only for the non-driving knee moment components ($M_{x'}$ and $M_{z'}$). Six complete pedaling cycles were used for each of the three models to compute the average load–angle curves for each subject. For each of the two simplified models, the root-mean-square difference (RMSD) from the complete spherical model was determined for each subject and for each of the two non-driving moment components. Both the $M_{x'}$ and $M_{z'}$ RMSD values were normalized for each subject by dividing them by the

respective peak varus moment and peak internal axial moment from the complete spherical joint model.

3. Results

The power stroke, defined as the region of the crank cycle when the applied knee flexion/extension moment is positive (i.e. tending to cause knee flexion), began at a crank angle of 306° and ended at a crank angle of 119° on average (Fig. 3). During the power stroke, the applied varus/valgus moment ($M_{x'}$) began valgus on average and became varus with a peak value of +6 N m at 70°, then decreased to 0 N m at the end of the power stroke. During the recovery stroke, defined as the region where the applied knee flexion/extension moment is negative, $M_{x'}$ became valgus with a peak value of –7 N m at an angle of 250°. During the power stroke, the applied internal/external axial moment ($M_{z'}$) was internal on average and peaked at +1 N m at 25°. The peak external axial moment of –2 N m occurred near the start of the recovery stroke.

The variability between subjects was quite large for both non-driving moments (Table 1). The peak applied varus moment ranged from –1.5 N m (maximum $M_{x'}$ value) to +19.6 N m. The peak applied valgus moment ranged from –3.4 to –13.5 N m. The coefficients of variability (CV) were 72.6% and 38.7% for the peak varus and valgus moments, respectively. $M_{z'}$ displayed similar variability between subjects where the peak internal axial moment ranged from 0.3 to 3.3 N m (CV of 59.9%) and the peak external axial moment ranged from 0.7 N m (minimum $M_{z'}$ value) to –5.3 N m (CV of 59.6%).

The crank angle locations of the peaks were similarly variable (Table 1). Although the peak varus moment occurred during the power stroke at a crank angle of approximately 70° (±10°) for the majority of the subjects (9 of 15), there were significant deviations from the average (CV of 67.5%). In contrast the crank angle corresponding to the peak valgus moment occurred during the recovery stroke and was more consistent (CV of 30.4%). Similarly, average crank angles for the peak internal axial moment (27.3°) occurred during the power stroke and were highly variable (CV of 157%) while the average crank angles for the peak external axial moment (174°) occurred during the recovery stroke and were more consistent (CV of 41.6%).

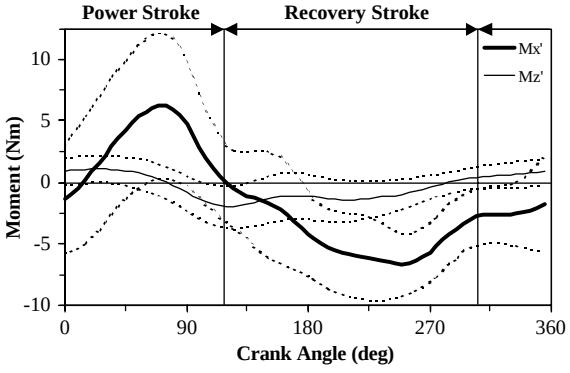

Fig. 3. Average non-driving varus/valgus ($+M_{x'}/-M_{x'}$) and internal/external axial ($+M_{z'}/-M_{z'}$) knee moments with ±1 S.D. envelopes for the 15 subjects used in this study. The power stroke began at a crank angle of 306° and ended at a crank angle of 119°.

Neglecting inertial contributions by the foot and shank out of the sagittal plane (i.e. simplified spherical joint model) led to differences in the non-driving moments from those of the complete spherical model primarily in the recovery stroke (Fig. 4). On average, during the power stroke, both the varus/valgus and internal/external axial moment patterns were similar between the two models after which the patterns began to diverge. The largest difference in peak values was in the peak valgus moment. The average RMSD for the 15 subjects was 2.0 N m for the varus/valgus moment, which was 11.9% of the peak varus moment determined by the complete spherical model (Table 2). For the axial moment curves, the average RMSD was 0.2 N m, which was 25.1% of the peak internal axial moment determined by the complete spherical model.

Adding the assumption of the revolute knee joint to the simplified spherical model (i.e. revolute joint model) led to results that were more different from those of the complete spherical model than the differences between the simplified spherical and complete spherical joint models (Fig. 4). On average, the varus/valgus moment curves from the revolute and complete spherical joint models typically exhibited similar patterns, but with large differences in peak values. The revolute joint model overestimated (in an absolute sense) both the peak varus and valgus moments by nearly 3 N m. The average RMSD between the varus/valgus curves of these two models for the 15 subjects was 4.1 N m, which was 23.9% of the peak varus moment determined using the complete spherical joint model (Table 2). These absolute and relative differences between the revolute and the complete spherical joint models were approximately twice the differences between the simplified spherical and complete spherical joint models.

The axial moments from the revolute joint model exhibited differences in both patterns and peak values from those of the complete spherical joint model. The revolute joint model overestimated the peak internal axial moment by nearly 1 N m where the crank angle of the peak occurred 145° later in the crank cycle (Fig. 4). The peak external axial moment was comparable between the models but occurred 40° earlier in the crank cycle for the revolute joint model. The average RMSD was 2.0 N m, which was 204% of the peak internal axial moment from the complete spherical joint model (Table 2). These absolute and relative differences

Table 1
Peak values of varus/valgus ($+M_{x'}/-M_{x'}$) and internal/external axial ($+M_{z'}/-M_{z'}$) moments and corresponding crank angles for all subjects used in this study

Subject	Peak $+M_{x'}$ (N m)	Peak $-M_{x'}$ (N m)	Peak $+M_{x'}$ angle (deg)	Peak $-M_{x'}$ angle (deg)	Peak $+M_{z'}$ (N m)	Peak $-M_{z'}$ (N m)	Peak $+M_{z'}$ angle (deg)	Peak $-M_{z'}$ angle (deg)
1	17.0	−9.4	75	195	1.0	−5.3	55	150
2	3.0	−6.2	70	260	1.2	−1.8	0	105
3	0.5	−8.8	310	230	0.4	−2.8	330	205
4	8.2	−6.4	75	255	1.7	−1.1	50	230
5	11.4	−5.9	55	225	2.1	−2.8	30	115
6	7.1	−7.6	85	260	0.9	−3.4	355	120
7	11.9	−12.5	25	215	3.3	−2.5	0	135
8	6.2	−8.4	155	270	0.3	−3.5	340	115
9	3.8	−11.7	70	255	1.8	0.7[a]	125	305
10	9.3	−4.4	70	195	1.9	−0.9	40	215
11	4.7	−8.7	40	235	1.3	−3.8	25	135
12	−1.5[b]	−10.9	60	235	2.2	−2.8	40	210
13	10.1	−3.4	70	260	3.1	−1.6	50	120
14	19.6	−13.5	75	180	0.6	−1.7	80	330
15	6.3	−3.8	130	0	0.9	−4.1	330	115
Average	7.8	−8.1	67.0	218.0	1.5	−2.5	27.3[c]	173.7
S.D.	5.7	3.1	45.2	66.3	0.9	1.5	42.9	72.3
C.V.(%)	72.6	38.7	67.5	30.4	59.9	59.6	157.0	41.6

[a] Minimum value for subject 9.
[b] Maximum value for subject 12.
[c] For values greater than 300, the average was computed after 360 was subtracted.

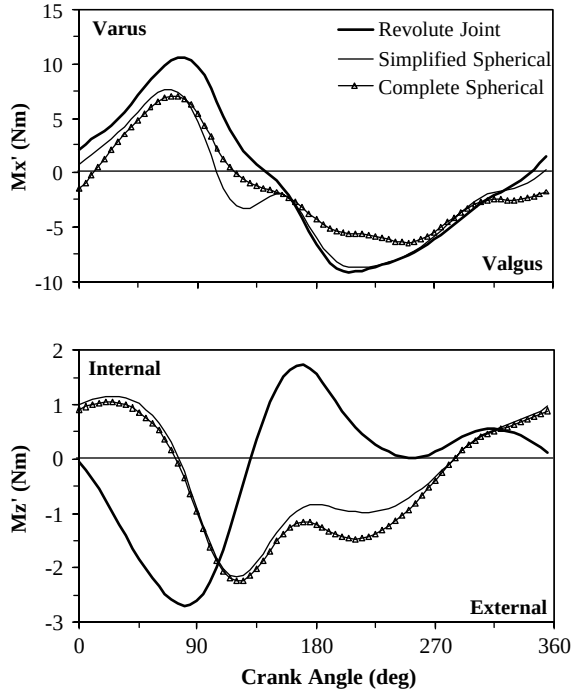

Fig. 4. Average varus/valgus ($+M_{x'}/-M_{x'}$) and internal/external axial ($+M_{z'}/-M_{z'}$) knee moments for the revolute joint, simplified spherical, and complete spherical models for the 15 subjects.

between the revolute and the complete spherical joint models were approximately ten times the differences between the simplified spherical and complete spherical joint models.

4. Discussion

Because over-use knee injuries are common in cycling, because non-driving intersegmental knee moment components are thought to be primarily responsible for the etiology of these injuries, and because no previous study known to the authors has determined these moment components with a complete 3-D model of the leg, one purpose of this study was to develop such a model and then use it to compute the moment components of interest. Another purpose was to justify the need for a complete 3-D model by comparing the results from this model to those from two simplified models. The key findings of this study were that on average a varus and internal axial moment must be resisted by musculoskeletal structures in the power stroke of the crank cycle while a valgus and external axial moment must be resisted in the recovery stroke; however, the variability between subjects was high. Also simplifying assumptions cause large differences in non-driving moments particularly when the knee joint kinematic model is considered to be revolute with the rotational axis perpendicular to the sagittal plane. Before discussing the importance of these findings several methodological issues should be reviewed critically to assess their potential to influence the findings of the study.

4.1. Methodological issues

Because of our interest in understanding the etiology of over-use injury and also in assessing the effectiveness

Table 2
Comparison of non-driving knee moments from the revolute joint (RJ), simplified spherical (SS), and complete spherical (CS) joint models. Root-mean-square difference (RMSD) values in N m and RMSD as a percentage of peak positive moment for both varus/valgus and internal/external axial moments are given

	Varus/Valgus				Internal/External Axial			
	RMSD (N m)		RMSD (% of peak + $M_{x'}$)		RMSD (N m)		RMSD (% of peak + $Mg_{x'}$)	
Subject	CS–SS	CS–RJ	CS–SS	CS–RJ	CS–SS	CS–RJ	CS–SS	CS–RJ
1	3.0	3.3	17.9	19.3	0.2	2.3	16.3	229.7
2	2.3	5.2	13.8	30.7	0.2	1.6	21.9	163.5
3	1.7	6.0	10.2	35.2	0.3	2.9	29.5	295.7
4	2.9	6.0	17.2	35.2	0.2	1.5	24.3	147.7
5	2.4	1.7	14.2	9.9	0.2	2.7	24.4	272.6
6	2.2	4.3	13.1	25.2	0.2	2.4	21.0	247.2
7	1.4	3.1	8.3	18.2	0.2	1.8	15.8	179.1
8	3.3	6.1	19.1	36.1	0.4	3.1	45.1	311.3
9	2.0	3.9	11.7	22.9	0.1	1.0	14.3	96.7
10	1.9	2.2	11.1	13.2	0.3	0.9	25.5	88.7
11	1.2	4.7	7.3	27.9	0.2	3.3	19.1	332.5
12	1.6	4.3	9.1	25.4	0.3	3.4	29.1	346.1
13	1.9	1.8	11.1	10.3	0.3	0.8	33.7	76.3
14	0.9	3.0	5.3	17.7	0.2	0.5	21.3	48.6
15	1.7	5.4	10.0	31.8	0.3	2.2	34.8	218.3
Average	2.0	4.1	11.9	23.9	0.2	2.0	25.1	203.6
S.D.	0.7	1.5	4.0	8.9	0.1	1.0	8.3	98.1

of different interventions to protect against over-use injury, a desirable goal of this study was to express knee loads in functionally meaningful directions (i.e. flexion/extension, varus/valgus, and internal/external axial). However, achieving this goal is difficult because the functional directions at the knee are neither orthogonal nor fixed to the femur or tibia (Grood and Suntay, 1983; Hollister et al., 1993). The functional flexion/extension axis is fixed to the femur, the internal/external rotation axis is fixed to the tibia, and the varus/valgus is a floating axis mutually perpendicular to the others. This presents a problem when expressing knee loads because the coordinate system needs to be fixed to one segment and should be orthogonal (Andrews, 1984). The coordinate system presented expresses knee loads in approximate functional directions, while satisfying these constraints. Defining a flexion/extension axis by projecting the flexion/extension axis onto a plane perpendicular to the long axis of the shank is reasonable considering that the angle of intersection between these two axes is nearly 90° (Hollister et al., 1993). While other coordinate systems exist for expressing knee loads (Cappozzo et al., 1995; Pennock and Clark, 1990; Ramakrishnan et al., 1987), our coordinate system expresses the loads in functionally and clinically meaningful directions.

One source of error that had the potential to affect the moment calculations was associated with the motion capture system. The error inherent to the motion capture system used in this study has been estimated on the order of 1–2 mm for both static and dynamic tests (Richards, 1999). Because these errors are composed of random, high frequency components which manifest as random noise (Cappozzo, 1991), the low-pass digital filtering operation as well as averaging of the data over multiple crank cycles reduced errors of this type.

Despite the fact the filtering operations reduced random errors, it is still possible that random noise introduced errors into the inertial loads computed with the complete spherical model. While it is difficult to quantitatively estimate errors in inertial loads due to random noise because this source of variation cannot be decoupled from natural physiological variation in generating the movement, evidence demonstrates that these errors were not substantial. All components of the linear and angular acceleration vectors demonstrated a repeatable pattern over time both within and across subjects. This pattern would not have been evident if the random errors were substantial in relation to these vector components.

A second source of error was movement of skin-mounted markers relative to underlying bone, which affects calculations of both segment kinematics and joint center positions. Marker movement has been shown to affect segment kinematics, where the magnitude of the error is location and task specific (Cappozzo et al., 1996; Fuller et al., 1997; Holden et al., 1997; Manal et al., 2000; Reinschmidt et al., 1997a; Reinschmidt et al., 1997b). A common result from these studies was that shank markers typically exhibit lower movement errors than thigh markers (Cappozzo et al., 1996; Reinschmidt

et al., 1997a). In addition, the effects of marker movement error on knee joint moments have been computed for walking where the shapes of the moment curves were largely unaffected but the averages were shifted, indicating systematic errors (Holden et al., 1997; Holden and Stanhope, 1998). Based on these observations and considering that the present study utilized only two skin-mounted shank markers (lateral malleolus and tibial tuberosity), marker movement was not an important source of error. Additionally, because the errors are expected to be systematic, conclusions can be drawn more confidently when relative changes are of interest, as was the case for the second objective of this study (Table 2). Likewise in assessing the effectiveness of methods for preventing over-use injury, this should not be an important source of error because changes in knee loads are the focus.

A final source of error was the placement of the markers for the static calibration trial. The static calibration procedure performed here established a quasi-functional tibia-fixed coordinate system based on the placement of the epicondyle and malleoli markers. These markers defined both the flexion/extension axis of the knee and the long axis of the tibia. Because the accuracy of the placement of these markers can affect the moments computed in the tibia-fixed reference frame (Ramakrishnan and Kadaba, 1991) and hence the repeatability of results between test days, it was of interest to estimate the error introduced into the non-driving moments from errors in marker placement.

To estimate these errors in the varus–valgus moment which is subject to the greater error, a Monte Carlo simulation was performed in which the x'-coordinate of each marker was varied according to a normal distribution with a zero mean and standard deviation (S.D.) of 1.9 mm. With this S.D., 99% of the distribution is contained within ± 5 mm which is the worst case error in the placement of an individual marker. From this simulation, the corresponding RMSE in the angle of both the x'- and y'-axis about the z'-axis was 1.2°. For a condylar width of 13 cm (average obtained from the static calibration trials of subjects) and a peak flexive moment of 45 N m (average obtained from the subjects), the RMSE introduced into the varus–valgus moment was 0.94 N m or 12% of the peak varus moment. Because the RMSE was 6 times smaller than the S.D. of the peak varus moment for the subjects, the variation between subjects evident in Table 1 was not strongly influenced by artifacts due to errors in marker placement. A similar conclusion holds for the axial moment because the RMSE due to errors in marker placement are much less than the RMSE for the varus/valgus moment.

Moreover, previous studies specifically aimed at examining repeatability in 3-D analysis of intersegmental loads also found that knee joint moments were repeatable between test days. Both Kadaba et al. (1989) and Growney et al. (1997) performed extensive investigations into the within-day and between-day repeatability of knee moments during walking. Both studies determined that the intersegmental knee moments were sufficiently repeatable between days to draw meaningful conclusions about kinetic measures such as knee moments from one data collection session.

4.2. Importance/interpretation of results

The first key result of this study was the large variability between subjects, indicating that the average non-driving moment curve does not represent the non-driving moment curve for an individual well, as indicated by the peak and peak angle quantities. While it is likely that some of the variability could be due to the error sources noted above, this result is consistent with observations of knee loads during both cycling (Boyd et al., 1997; Ruby et al., 1992a; Ruby et al., 1992b) and walking (Andriacchi and Strickland, 1985; Li et al., 1993; Ramakrishnan et al., 1987). This result is important in developing a technology to prevent over-use injury because subject-to-subject variability may complicate assessing how an intervention affects the inter-segmental knee loads. Consequently, the effect of any intervention should be examined on a subject-by-subject basis.

The causes for the high inter-subject variability observed in cycling have been attributed to subject-specific anatomy and equipment set-up (Holmes et al., 1994; Ruby et al., 1992b). Approximately 60% of the variability in the non-driving knee moments can be attributed to specific lower limb anatomical measures (Ruby et al., 1992b). Equipment set-up parameters such as saddle height, saddle position, bicycle frame geometry, shoe type and shape, and cleat positioning are also potential sources of variability. The variability that was observed in this study is likely due to both of these factors, because the riding position was not standardized and the subject anatomy was not screened.

The result that non-driving knee moments were substantial during pedaling could be important in understanding the etiology of over-use cycling injuries (Ruby et al., 1992a). The combined loads that are developed (i.e. flexor/extensor with varus/valgus and internal/external axial moments) must be supported by structures crossing the knee. If knee joint musculature is responsible for supporting these combined loads, then over-use injuries could develop. Chondromalacia patellae, which is a common over-use injury in cyclists (Holmes et al., 1991), is one example. The vastus lateralis has a moment arm about the varus/valgus axis of the knee along with its primary moment arm about the flexion/extension axis (Buchanan et al., 1996; Lloyd and Buchanan, 1996). The development of a large varus

knee moment during the power stroke could cause an increase in the force output of the vastus lateralis to equilibrate this load. This preferential force production could in turn cause a muscular imbalance in the quadriceps, affecting patellar tracking and increasing patellar contact pressures, leading to patello-femoral pain (Wolchok et al., 1998).

Used to generate the simplified spherical model, the assumption that the medial/lateral component of acceleration and moments of inertia about the x^* and z^* principal axes for the foot and shank were zero resulted in reasonably good predictions of both the timing and peak values of the non-driving knee moments (Fig. 4, Table 2). The divergence during the recovery stroke occurred because the relative contributions of the inertial loads increased relative to the contributions from the pedal forces, which decreased considerably in this region of the crank cycle. These results indicate that, while introducing differences into the computations of the non-driving knee moments, the assumptions of the simplified spherical model introduce less differences in non-driving moments in the power stroke than in the recovery stroke.

The pronounced differences between the complete spherical joint model and the revolute joint model (Fig. 4, Table 2) occurred because of the combined effects of the assumption noted above for the simplified spherical model in conjunction with the additional assumption that the flexion/extension axis y' remains coincident with the laboratory y-axis which was perpendicular to the sagittal plane. For the varus/valgus moment each assumption contributed equally to the RMSD (Table 2) but for the axial moment, the second assumption contributed about ten times more to the RMSD than the first assumption. Because the second assumption contributed so much more to the RMSD than the first assumption for the axial moment, it can be concluded that the major difference between the complete spherical joint model and the revolute joint model is due to the difference in the orientation of the two local tibial coordinate systems. As noted earlier, the non-driving moments are sensitive to the coordinate system in which they are expressed because the flexion/extension moment is much larger than the non-driving moments.

This point can be illustrated further by examining the difference in the axial moment due to the difference in orientation of the y'–z' axes for the spherical joint model relative to the revolute joint model. Averaging over the subjects, the mean difference in orientation was 2.7° and ranged from 5.3° valgus to −0.5° varus during one crank cycle. For a peak flexive moment of 45 N m, a 2.7° rotation of the $y'-z'$ axes results in a 2.1 N m difference in the axial moment computed using the revolute joint model. As explained in the Methodological Issues subsection, the axial moments for the complete spherical model were repeatable with substantially less error than 0.9 N m which was the error computed for the varus–valgus moment. Accordingly, the revolute joint model introduced differences into the axial moment that far exceeded the errors in the axial moment determined using the complete spherical model.

Because the different coordinate systems yield differences in the load components that are substantial enough to affect the interpretation of over-use injury mechanisms particularly in the case of internal/external axial moments (Fig. 4), one question that remains is which is the more appropriate coordinate system. The answer to this question depends on the purpose of the model. If understanding the etiology of over-use knee injury is the purpose, then it would be advantageous to compute the knee load components in a subject-specific coordinate system that provides clinically meaningful loading variables. In ignoring axial rotation, which is a degree of freedom inherent to the knee joint (Hollister et al., 1993), the revolute joint model necessitates a coordinate system that is not truly fixed to the shank and hence is not subject specific. In allowing three degrees of rotational freedom, the spherical knee model enables a coordinate system that reflects subject-specific 3-D rotations of the shank including axial rotation. Hence this coordinate system should provide a more meaningful representation of the loads that must be born by the structures crossing the knee that are susceptible to over-use injury.

Acknowledgements

The authors are grateful to the Whitaker Foundation for providing the funds to purchase the motion analysis system.

References

Andrews, J.G., 1984. On the specification of joint configurations and motions. Journal of Biomechanics 17, 155–158.

Andriacchi, T.P., Strickland, A.B., 1985. Gait analysis as a tool to assess joint kinetics. In: Berme, N., Engin, A.E., Correia Da Silva, K.M. (Eds.), Biomechanics of Normal and Pathological Human Articulating Joints. NATO SI Series. Martinus Nijhoff, Dordrecht.

Boyd, T.F., Neptune, R.R., Hull, M.L., 1997. Pedal and knee loads using a multi-degree-of-freedom pedal platform in cycling. Journal of Biomechanics 30, 505–511.

Buchanan, T.S., Kim, A.W., Lloyd, D.G., 1996. Selective muscle activation following rapid varus/valgus perturbations at the knee. Medicine and Science in Sports and Exercise 28, 870–876.

Cappozzo, A., 1991. Three-dimensional analysis of human walking: experimental methods and associated artifacts. Human Movement Science 10, 589–602.

Cappozzo, A., Catani, F., Croce, U.D., Leardini, A., 1995. Position and orientation in space of bones during movement: anatomical frame definition and determination. Clinical Biomechanics 10, 171–178.

Cappozzo, A., Catani, F., Leardini, A., Benedetti, M.G., DellaCroce, U., 1996. Position and orientation in space of bones during movement: experimental artefacts. Clinical Biomechanics 11, 90–100.

Davis, R.R., Hull, M.L., 1981. Measurement of pedal loading in bicycling: II. Analysis and results. Journal of Biomechanics 14, 857–872.

de Leva, P., 1996. Adjustments to Zatsiorsky–Seluyanov's segment inertia parameters. Journal of Biomechanics 29, 1223–1230.

Ericson, M.O., Nisell, R., Ekholm, J., 1984. Varus and valgus loads on the knee joint during ergometer cycling. Scandinavian Journal of Sports Sciences 6, 39–45.

Francis, P.R., 1986. Injury prevention for cyclists: a biomechanical approach. In: Burke, E. (Ed.), Science of Cycling. Human Kinetics, Champaign, IL.

Fuller, J., Liu, L.J., Murphy, M.C., Mann, R.W., 1997. A comparison of lower-extremity skeletal kinematics measured using skin- and pin-mounted markers. Human Movement Science 16, 219–242.

Grood, E.S., Suntay, W.J., 1983. A joint coordinate system for the clinical description of three-dimensional motions: application to the knee. Journal of Biomechanical Engineering 105, 136–144.

Growney, E., Meglan, D., Johnson, M., Cahalan, T., An, K-N., 1997. Repeated measures of adult normal walking using a video tracking system. Gait and Posture 6, 147–162.

Holden, J.P., Orsini, J.A., Siegel, K.L., Kepple, T.M., Gerber, L.H., Stanhope, S.J., 1997. Surface movement errors in shank kinematics and knee kinetics during gait. Gait and Posture 5, 217–227.

Holden, J.P., Stanhope, S.J., 1998. The effect of variation in knee center location estimates on net knee joint moments. Gait and Posture 7, 1–6.

Hollister, A.M., Jatana, S., Singh, A.K., Sullivan, W.W., Lupichuk, A.G., 1993. The axes of rotation of the knee. Clinical Orthopaedics and Related Research, 259–268.

Holmes, J.C., Pruitt, A.L., Whalen, N.J., 1991. Cycling knee injuries. Cycling Science 3, 11–14.

Holmes, J.C., Pruitt, A.L., Whalen, N.J., 1994. Lower extremity overuse in bicycling. Clinics in Sports Medicine 13, 187–205.

Kadaba, M.P., Ramakrishnan, M.E., Wootten, J., Gorton, G., Cochran, G.V.B., 1989. Repeatability of kinematic, kinetic, and electromyographic data in norrmal adult gait. Journal of Orthopedic Research 7, 849–860.

Li, J., Wyss, U.P., Costigan, P.A., Deluzio, K.J., 1993. An integrated procedure to assess knee-joint kinematics and kinetics during gait using an optoelectric system and standardized X-rays. Journal of Biomedical Engineering 15, 392–400.

Lloyd, D.G., Buchanan, T.S., 1996. A model of load sharing between muscles and soft tissues at the human knee during static tasks. Journal of Biomechanical Engineering 118, 367–376.

Manal, K., McClay, I., Stanhope, S., Richards, J., Galinat, B., 2000. Comparison of surface mounted markers and attachment methods in estimating tibial rotations during walking: an in vivo study. Gait and Posture 11, 38–45.

Pennock, G.R., Clark, K.J., 1990. An anatomy-based coordinate system for the description of the kinematic displacements in the human knee. Journal of Biomechanics 23, 1209–1218.

Ramakrishnan, H.K., Kadaba, M.P., 1991. On the estimation of joint kinematics during gait. Journal of Biomechanics 24, 969–977.

Ramakrishnan, K.K., Kadaba, M.P., Wootten, M.E., 1987. Lower extremity joint moments and ground reaction torque in adult gait. In: Stein, J.L. (Ed.), Biomechanics of Normal and Prosthetic Gait. ASME, New York.

Reinschmidt, C., van den Bogert, A.J., Nigg, B.M., Lundberg, A., Murphy, N., 1997a. Effect of skin movement on the analysis of skeletal knee joint motion during running. Journal of Biomechanics 30, 729–732.

Reinschmidt, C., van den Bogert, A.J., Lundberg, A., Nigg, B.M., Murphy, N., Stacoff, A., Stano, A., 1997b. Tibiofemoral and tibiocalcaneal motion during walking: external vs. skeletal markers. Gait and Posture 6, 98–109.

Richards, J.G., 1999. The measurement of human motion: a comparison of commercially available systems. Human Movement Science 18, 589–602.

Ruby, P., Hull, M.L., 1993. Response of intersegmental knee loads to foot/pedal platform degrees of freedom in cycling. Journal of Biomechanics 26, 1327–1340.

Ruby, P., Hull, M.L., Hawkins, D., 1992a. Three-dimensional knee joint loading during seated cycling. Journal of Biomechanics 25, 41–53.

Ruby, P., Hull, M.L., Kirby, K.A., Jenkins, D.W., 1992b. The effect of lower-limb anatomy on knee loads during seated cycling. Journal of Biomechanics 25, 1195–1207.

Winter, D.A., 1990. In Biomechanics and Motor Control of Human Movement. Wiley, New York.

Wolchok, J.C., Hull, M.L., Howell, S.M., 1998. The effect of intersegmental knee moments on patellofemoral contact mechanics in cycling. Journal of Biomechanics 31, 677–683.

Zatsiorsky, V.M., Seluyanov, V.N., Chugunova, L.G., 1990. Methods of determining mass-inertial characteristics of human body segments. In: Chernyi, G.G., Regirer, S.A. (Eds.), Contemporary Problems of Biomechanics. CRC Press, Massachusetts, pp. 272–291.